Research Letters

Electronic Structure and Infrared Light Emission in Dislocation-Engineered Silicon

Cheng-Lun Hsin, Hsu-Shen Teng, Hsiang-Yuan Lin, Tzu-Hsuan Cheng, Chao-Chia Cheng, and Po-Liang Liu

***Abstract*—One of the perspectives of the Si-based technology is the optical interconnect for data transmission and applications in optoelectronic integrated circuit. In this report, the engineered dislocation network was proposed, and the atomic structure of the dislocation array was revealed by high-resolution transmission electron microscope and scanning tunneling microscope. The photoluminescence emission is strong and compatible with intrinsic Si characteristic peak, making it possible as light emitters in silicon. The analysis of dislocation array-induced scanning tunneling spectroscopy identified the presence of defect levels under the conduction band, compared with the occupied and unoccupied Kohn–Sham orbitals in the forbidden gap of Si derived from first-principles theoretical models. This study demonstrated the possibility of dislocation-induced optical transition from a theoretical and experimental perspective, which will be essential in the development of Si-based optoelectronic integrated circuit.**

***Index Terms*—Density of state, dislocation array, first-principles calculations, network, photoluminescence, tunneling current.**

I. Introduction

THE Si-based integrate circuit (IC) design and fabrication has been the primary industry since the 20th century. Recently, IC technologies for integrating optoelectronic devices and electronic circuitry, the so-called optoelectronic IC [1], [2], present problems in the operation speed limited by the resistive-capacitive delay and the miniaturization of the Cu interconnect [3], [4]. Desirable key properties for the Si-based IC are the optical data transmission and applications in optoelectronic IC [5], [6]. The optical absorption, transmission, and emission in semiconductor devices rely on materials having direct bandgaps. Unfortunately, silicon is an indirect bandgap material. One way of overcoming the difficulties of producing silicon-based light-emitting IC is the semiconducting metal silicides [7]. An alternative way of producing silicon-based photonic IC is the defect engineered Si sub-bandgap light-emitting diodes. In this regard the band-to-band and defect luminescence at room temperature has been demonstrated experimentally in a phosphorus doped n-type on a boron doped p-type Si films with crystal defects/dislocations [8], [9]. However, the phonon-assisted recombination in Si nanocrystals exhibits an exponential decay at a small excitation power, which degrades the internal quantum efficiency of the photoluminescence (PL) [10]. On the other hand, the radiative recombination of electrons in the metal gate electrode and holes at the dislocation related states has attracted much attention in the metal-oxide-silicon tunneling structure based on the dislocation network in direct silicon bond wafer [11]. The dislocation related luminescence at room temperature is acquired to obtain 1.5 μm emission wavelength, about ten times larger than the band-to-band luminescence [12]. Recently, we have developed the dislocation networks by bonding two (0 0 1) silicon wafers (the Si bicrystal) with the twist angle between both wafers [13]. The Si bicrystals are used as templates for subsequent growth of titanium silicide nanostructures. The dislocation networks with respect to the induced surface strain are likely to promote the stepwise growth of the titanium silicide nanorods rather than nanoclusters with random shapes. Very recently, the subsequent work in the dislocation networks by bonding (0 0 1), (1 1 1), and (1 1 0) silicon wafers with (0 0 1) silicon-on-insulator (SOI) wafers was shown to display the tunable dislocation spacing of the network [14]. In this report, we expand this study by analyzing the electronic properties and providing the mechanism of PL emission in the dislocation engineered silicon, as demonstrated by first-principles theoretical studies. First of all, the dislocation networks by bonding (0 0 1) silicon wafers with (0 0 1) SOI wafers are fabricated and revealed by a high-resolution transmission electron microscopy (HRTEM) and scanning tunneling microscopy (STM). Second, we measure the PL of the dislocation related luminescence at room temperature. Third, the scanning tunneling spectroscopy

Manuscript received April 27, 2014; revised February 21, 2015; accepted February 24, 2015. Date of publication March 9, 2015; date of current version May 6, 2015. The review of this paper was arranged by Associate Editor N.-C. Panoiu. This work was supported by the Ministry of Science and Technology, Taiwan, under Grant MOST 103-2633-E-008-001, and in part by the Norwegian Research Council. Computational studies were performed using the resources of the National Center for High Performance Computing. Scanning tunneling microscopy was technologically supported by Omicron. *(Corresponding author: Cheng-Lun Hsin)*

C.-L. Hsin and H.-S. Teng are with the Department of Electrical Engineering, National Central University, Chongli 32001, Taiwan (e-mail: clhsin@ee.ncu.edu.tw; yso9197ce@hotmail.com).

H.-Y. Lin is with the Graduate Institute of Precision Engineering, National Chung Hsing University, Taichung 402, Taiwan (e-mail: HYLin15@winbond.com).

T.-H. Cheng and C.-C. Cheng are with the Department of Physics, National Central University, Chongli 32001,Taoyuan, Taiwan (e-mail: jetx1110@gmail.com; saujia@cc.ncu.edu.tw).

P.-L. Liu is with the Graduate Institute of Precision Engineering, National Chung Hsing University, Taichung 402, Taiwan, and also with the Department of Physics, Norwegian University of Science and Technology, N-7491 Trondheim, Norway (e-mail: pliu@dragon.nchu.edu.tw).

Color versions of one or more of the figures in this paper are available online at http://ieeexplore.ieee.org.

Digital Object Identifier 10.1109/TNANO.2015.2411292

1536-125X © 2015 IEEE. Personal use is permitted, but republication/redistribution requires IEEE permission.
See http://www.ieee.org/publications_standards/publications/rights/index.html for more information.

(STS) is used to provide the current–voltage (*I–V*) and the normalized differential conductance-voltage (d*I*/d*V*)/(*I*/*V*) characteristics of the dislocation networks. Finally, we performed *ab initio* calculations to elucidate the PL spectrum with respect to the twist–bonded dislocation network. This study demonstrated that the electronic structure of the dislocation network will be essential in the development of Si-based optoelectronic IC.

II. Experiment

The (0 0 1) silicon wafers and (0 0 1) SOI wafers with a top silicon layer approximately 30 nm thick were cleaned using the standard Radio Company of America process to remove residual organic and metallic contaminants and then dipped in an dilute HF solution to hydrogen passivate their surface prior to the wafer bonding. The dislocation networks was fabricated by twist wafer bonding (0 0 1) silicon wafers with (0 0 1) SOI wafers at the annealing temperature of 1100 °C for 1 h. The silicon substrate and buried oxide layer of the SOI wafers were then removed by the mechanical grinding and chemical etching in KOH solution. Thus, a thin Si layer (∼20 nm) was transferred and dislocation arrays were formed at the bonding interface. The transferred top silicon layers have to be thinned down for the measurement of the tunneling current between the STM tip and surface-terminated dislocations. The twist-bonded (0 0 1) layers were immersed in piranha solution (H_2SO_4:H_2O_2 = 4:1) to oxidize Si surface and in dilute HF to remove surface oxides using a sequence of four 5 min cycles of heating at 85 °C, which lead to a thin residual top silicon layer of the SOI wafers (∼1 nm) on (0 0 1) silicon wafers. The thin twist-bonded (0 0 1) layers were then annealed at 600 °C for 12 h and subsequently flashed to 1200 °C for 60 s at 2×10^{-9} torr for the purpose of surface reconstruction and removing any residual surface contaminants, respectively. STS was measured in Omicron STM1 and HRTEM (JEOL-2100F) was performed to image the atomic structure. The HRTEM images calculated using the fast Fourier transform algorithm and STM/STS measurements at room temperature indicate the structural and electronic properties of the dislocation networks. The PL measurements were performed through Ar laser operating at a 514.5 nm wavelength with 100 mW of output power at 80 °K and confirm the presence of dislocation array-induced levels. Our experimental results are further supported by first-principles theoretical calculations of the PL defect-peck of the dislocation network.

III. Result and Discussion

Fig. 2(a) is the schematic illustration of the (0 0 1) Si atomic arrangement. A twist angle between these two layers would result in an orthogonal network, which are along the [2 2 0] and [$\bar{2}$ 2 0] directions. The HRTEM image of Si with dislocation network is depicted in Fig. 2(b). With no interference of the miscut dislocations [15], the network is well arranged. The arrow in (b) is analogous to that in the schematic figure, highlighted the area where the atomic arrangement is distorted by the dislocation intersection. The white lines (denoted as "c" and "d") in Fig. 1(b) featured equivalent atomic (2 2 0) planes across the dislocation. A small mismatch between "c" and "d" can be directly imaged,

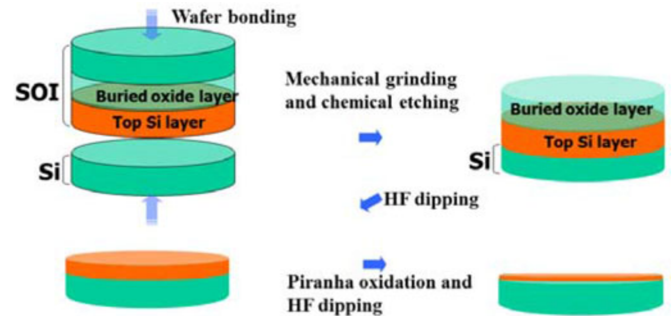

Fig. 1. The schematic illustration of the sample fabrication process.

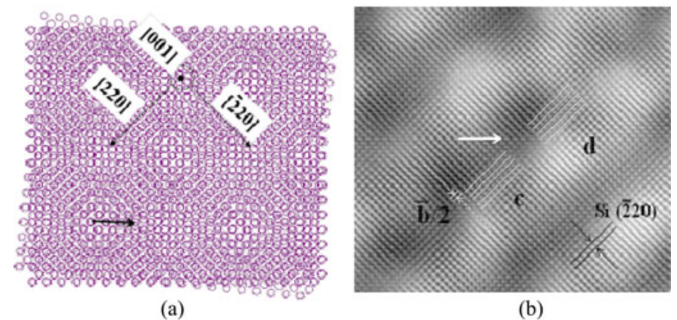

Fig. 2. (a) Schematic illustration of the (0 0 1) Si atomic arrangement. A misorientation angle between these two layers results in the orthogonal dislocation network along the [2 2 0] direction. (b) HRTEM image of Si with dislocation network. The white lines highlighted the (2 2 0) planes across the dislocation intersection pointed with a white arrow.

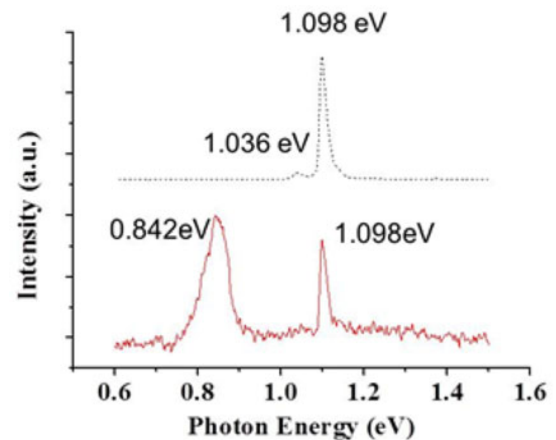

Fig. 3. PL of the (0 0 1) Si substrate (top, black-dashed line) and (0 0 1) Si substrate with dislocation array (bottom, red-solid line).

which is half of the Burgers vector of the screw dislocation on (2 2 0) plane.

Dislocation array may function as a recombination center in Si, analogous to an active layer of light emitting devices. Fig. 3 demonstrated that the infrared luminescence is strongly dependent on the dislocation network since the red-solid spectrum of Si with dislocation array exhibits a strong infrared emission at 0.842 eV, rather than that of blank Si (black-dashed line).

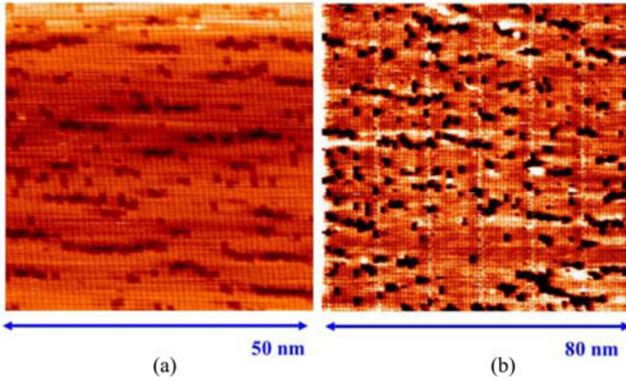

Fig. 4. STM images of (a) Standard Si (0 0 1)-(2 × 1) reconstruction and (b) Si (0 0 1)-(2 × 1) reconstruction with dislocation array exposed to the surface.

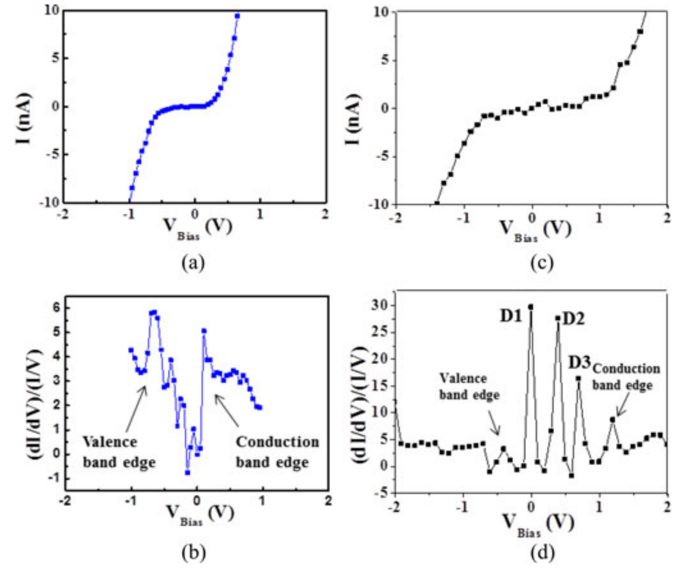

Fig. 5. Correlation of DOS and dislocation networks. (a) STS *I–V* measurement and (b) the normalized conductance (d*I*/d*V*)/(*I*/*V*) of the Si substrate. (c) STS *I–V* measurement and (d) the normalized conductance (d*I*/d*V*)/(*I*/*V*) of the Si substrate with dislocation array.

Moreover, the luminescence spectra of different dislocation interspacings (from 2 to 80 nm, not shown here) displayed similar emission characteristics. To consider the absorption depth of excitation source ($\sim 1\ \mu$m in depth for lightsource of 514.5 nm in wavelength) and PL quantum efficiency of Si, the luminous efficiency of this two-dimensional (2-D) network should be very high. Previous report has demonstrated 1% of the electroluminescence efficiency at room temperature [12], suggesting that the dislocation engineering of this 2-D network can be an efficacious way to generate luminescence. (0 0 1) Si substrate and (0 0 1) Si with dislocation array exposed to the surface were both investigated in the STM, and the images were revealed in Fig. 4(a) and (b), respectively. Because of the ultra-high vacuum and the preparation process, standard Si(0 0 1)-(2 × 1) reconstruction [16] was presented with rows of dimers. The surface of the Si is not perfect with rows of defects. These long and straight defects, occasionally with kinks, are the typical "A-type" steps [17], which can also be found in the samples with dislocation array, as well as the Si(0 0 1)-(2 × 1) reconstruction. Nevertheless, the orthogonal network was also detected per 13 rows of dimers, indicating dislocation array with interspacing of 13.2 nm. The STM tip positioned on the top region of the dislocation array was ~0.01 nm higher, prompting the tunneling from the tip to the top of the dislocation array. This result suggested that the dislocation array could have influence on the electronic defect level distribution in the bandgap. Recently, the condensation of 2-D oxide-interfacial charges into 1-D electron chains by the misfit-dislocation strain field was reported [18]. Our STM image has responded their results that the dislocation line can be revealed by the scanning tunneling current with higher charge density condensed on the dislocation array.

The standard current–voltage characteristics of (0 0 1) Si and (0 0 1) Si with dislocation array by STS were shown in the Fig. 5(a) and (c), respectively. Form the *I–V* measurement, a larger current appeared in the positive bias for the Si substrate, while in the negative bias for the sample with dislocation array when the bias is applied on the tip. This behavior indicates that the charge transport in the valence band is much larger than in the conduction band for sample with dislocation array due to the p-type SOI [19]. To consider the dependence of the tip-sample separation and the bias, the normalized conductance (d*I*/d*V*)/(*I*/*V*) is a better representative of the density of states (DOS) than the differential conductance (d*I*/d*V*) [20]. The features of normalized conductance of Si without and with dislocation array are depicted in Fig. 5(b) and (d), respectively. For the case of blank Si, there is a change in the surface states, yielding small amount of states in the bandgap, which may be due to the dimer or dimer vacancies. For the spectrum of the Si with dislocation array, several sharp peaks were observed with the increase of the bias, whereas remaining a constant plateau at negative bias. This rectifying *I–V* curve in Fig. 5(a) is representative in the STS, and the normalized conductance in Fig. 5(b) that shows a sharp increase corresponds to conduction band edge and valence band edge of the surface. In our experiments, if the tungsten tip of the STM is not close to the sample surface, the magnitude of noise of the *I–V* measurement is usually on the order of several hundreds of femto-ampere, which is much lower than the tunneling current that we measured. Thus, we believe that the thermal noise in Fig. 5(c) and (d) is negligible and the sharp peaks in the measured *I–V* curve that present in the bandgap contain the information of the dislocation-induced defect level, rather than thermal noise. According to the theory for the DOS calculation, a sharp peak followed by a non-zero flat plateau usually represents a band edge, whereas abrupt sharp peaks (denoted as D1, D2, and D3) depicted the defect levels in the bandgap. Thus, our experimental results clearly identified that there are about three dislocation induced defect levels near the conduction band edge, which could contribute to the infrared emission of our PL result. These experimental peaks have vast amounts in height and drops back to zero, similar to the Van Hove singularities [21], [22], where $d[g(E)]/dE$ diverges in a 3-D solid and play important roles in optical intensity. Moreover, the measured band edge difference for the silicon with dislocation array is larger than that of intrinsic Si substrate.

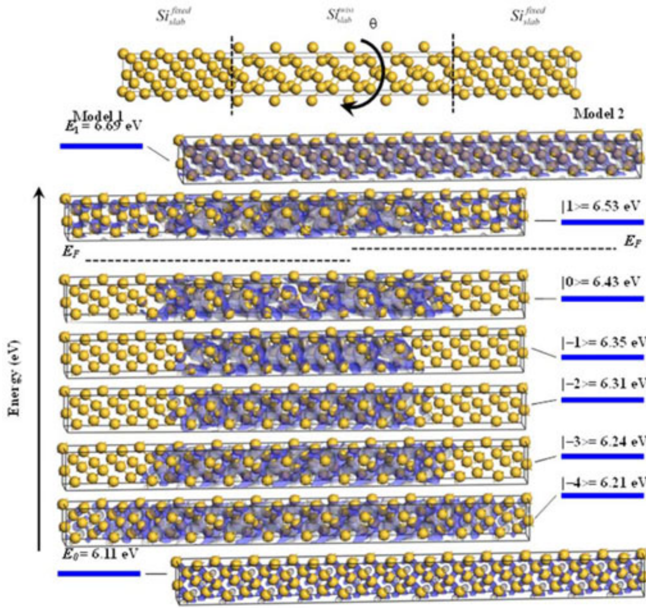

Fig. 6. Top panel: schematic illustration of the twist–bonded interfacial concept for Si (gold spheres) alloys. The $\boldsymbol{Si}_{\rm slab}^{\rm twist}$ slab has been rotated via the twist angle θ with respect to the $\boldsymbol{Si}_{\rm slab}^{\rm fixed}$ slab. Bottom panel: HOMO and LUMO isosurfaces of Models 1 and 2 arranged by energy and denoted by the shade of blue.

In the PL spectrum, the emission only comes from the transition of intrinsic Si bandgap and the dislocation-induced defect level. This result suggested that the band-to-band transition of the Si with dislocation array could be still indirect. According to atomic structure of a dislocation network within a 3-D Si lattice, the atoms of the network should be connected with dangling bonds. These defects and lattice irregularities around the dislocation core are known to cause states in the bandgap of Si between the valence and conduction band. For our case of a p-type SOI wafer, the dislocation-related states can be occupied with holes and form a positive line of charges, depending on the impurity and doping of the Si wafer [23]. Due to the space charge neutrality and electrostatics, the positively charged dislocation lines would be enclosed with negatively charged ions. As the consequence, the distribution of the space charges results in the bending of the conduction and valence band, and the appearance of defect level in the forbidden bandgap. To further clarify PL defect-peak of the dislocation network, we adopt a series of 96-atom Si crystallographic cells (24 monolayers) of the tetragonal lattice structure constructed using basic cubic Si unit cells. The twist–bonded interfaces are modeled as a superlattice consisting of 12 monolayers of the Si slab rotated a twisting angle about its c axis denoted by $\boldsymbol{Si}_{\rm slab}^{\rm twist}$ and the other 12 monolayers of the Si slab fixed at correct atomic geometries denoted by $\boldsymbol{Si}_{\rm slab}^{\rm fixed}$. Subsequently, the two equivalent interfaces are obtained after both slabs, the $\boldsymbol{Si}_{\rm slab}^{\rm fixed}$ and $\boldsymbol{Si}_{\rm slab}^{\rm twist}$ slab, have been rotated with respect to each other with twist angles θ as shown in Fig. 6. Two interface competitive models with misorientations of 0° and 6° were studied in detail by conducting first-principles density functional theory (DFT) calculations using the Cambridge serial total energy package [24], [25], correspond to Models 1 and 2, respectively. This code employs ultrasoft pseudopotentials [26] and a plane-wave basis to treat the electronic structure within the PW 91 generalized gradient approximation [27], [28]. The convergence of electronic properties was achieved with a plane wave cutoff of 120 eV and a $4 \times 4 \times 1$ Monhorst-Pack grid in the first Brillouin zone to achieve a force accuracy of 0.1 eV/Å. To elucidate the electronic property at both Models we examined the highest occupied Kohn–Sham orbitals (HOMO) and lowest unoccupied Kohn–Sham orbitals (LUMO) as displayed in Fig. 6. We clearly see that the HOMO levels of Model 1 are localized on the midpoint positions between two atoms as localized bond charge pockets (E_0 valence band), which are referred to as the *sp*^{3}-hybridized orbitals bonding band. The LUMO isosurfaces are significantly different from the HOMO isosurfaces in Model 1. The LUMO levels are not only around Si atoms but also occupied Si–Si bonds (E_1 conduction band), which are referred to as *sp*^{3}-hybridized orbitals antibonding band. In the case of Model 2, dislocation-related states, |1>, |0>, |–1>, |–2>, |–3>, and |–4> levels, can be occupied orbitals around Si atoms in the forbidden gap of the non-twist-bonded Si slab between the valence E_0 and conduction E_1 band (Model 1). Thus, |0>, |–1>, |–2>, |–3>, and |–4> levels are filled by electrons depends on the Fermi energy ($E_{\rm F}$, dashed-dotted line in Fig. 6). Our |0>, |–1>, |–2>, and |–3> isosurfaces show that the spatial distribution of localized orbitals exists in the $\boldsymbol{Si}_{\rm slab}^{\rm twist}$ slab. In order to compare with the experimental PL observations the fundamental gap between the conduction band and defect levels can be corrected with a "scissor operator" to match the PL peaks due to the well-known bandgap underestimation of DFT calculations. The gap between the E_0 valence and E_1 conduction bands (6.11–6.69 eV as shown in Fig. 6) is corrected by multiplying a scissor correction of 1.893 to approach the PL emission in the 1.098 eV spectral region (see Fig. 3). Our corrected gap between E_1 conduction bands and dislocation-related state |–3> is 0.852 eV, closely matching the PL defect-peak of the twist–bonded dislocation network (0.842 eV). Note the excellent agreement between the experimental and simulated results suggest a possible explanation for the defect-related peak in PL of the twist–bonded dislocation network due to the dislocation-related orbitals bonding band.

IV. Conclusion

In conclusion, we have revealed the atomic structure and characteristics of the dislocation arrays from a theoretical and experimental perspective. The analysis of tunneling current and STS identified that the dislocation array induced three defect levels under the conduction band, which could contribute to defect level transition. PL of infrared emission was measured, and the result proves that Si substrate with dislocation array has the potential in light emitting for future optical communications. First-principles calculations confirm the influence of the dislocation-related defect levels, which are consistent with our PL and STS results. This study demonstrated the dislocation-induced optical transition and expanded the application of engineered-dislocations, which will be essential in the development of Si-based optoelectronic IC.

References

[1] K. W. Lee, A. Noriki, K. Kiyoyama, T. Fukushima, T. Tanaka, and M. Koyanagi, "Three-dimensional hybrid integration technology of CMOS, MEMS, and photonics circuits for optoelectronic heterogeneous integrated systems," *IEEE Trans. Electron Devices*, vol. 58, no. 3, pp. 748–757, Mar. 2011.

[2] D. Saha, D. Basu, and P. Bhattacharya, "A monolithically integrated magneto-optoelectronic circuit," *Appl. Phys. Lett.*, vol. 93, no. 19, pp. 194104-1–194104-3, Nov. 2008.

[3] Y. Furukawa, H. Yonezu, A. Wakahara, S. Ishiji, S. Y. Moon, and Y. Morisaki, "Growth of Si/III-V-N/Si structure with two-chamber molecular beam epitaxy system for optoelectronic integrated circuits," *J. Cryst. Growth*, vol. 300, no. 1, pp. 172–176, Mar. 2007.

[4] H. Y. Yu, J. H. Park, A. K. Okyay, and K. C. Saraswat, "Selective-area high-quality germanium growth for monolithic integrated optoelectronics," *IEEE Electron Device Lett.*, vol. 33, no. 4, pp. 579–581, Apr. 2012.

[5] A. A. Ketterson, J. W. Seo, M. H. Tong, K. L. Nummila, J. J. Morikuni, K. Y. Cheng, S. M. Kang, and I. Adesida, "A MODFET-based optoelectronic integrated-circuit receiver for optical interconnects," *IEEE Trans. Electron Devices*, vol. 40, no. 8, pp. 1406–1416, Aug. 1993.

[6] Y. K. Fang, C. R. Liu, K. H. Chen, and C. H. Lin, "A low-cost and high-current gain a-Si/C-Si heterojunction photoreceiver for large-area optoelectronics integrated-circuit applications," *IEEE Electron Device Lett.*, vol. 16, no. 5, pp. 190–192, May 1995.

[7] D. Leong, M. Harry, K. J. Reeson, and K. P. Homewood, "A silicon/iron-disilicide light-emitting diode operating at a wavelength of 1.5 mu m," *Nature*, vol. 387, no. 6634, pp. 686–688, Jun. 1997.

[8] M. Kittler, T. Arguirov, A. Fischer, and W. Seifert, "Silicon-based light emission after ion implantation," *Opt. Mater.*, vol. 27, no. 5, pp. 967–972, Feb. 2005.

[9] W. L. Ng, M. A. Lourenco, R. M. Gwilliam, S. Ledain, G. Shao, and K. P. Homewood, "An efficient room-temperature silicon-based light-emitting diode," *Nature*, vol. 410, no. 6825, pp. 192–194, Mar. 2001.

[10] T. Puritis and J. Kaupuzs, "Radiative phonon-assisted and Auger recombination in Si nanocrystals," *Opt. Mater.*, vol. 32, no. 8, pp. 840–844, Jun. 2010.

[11] X. Yu, W. Seifert, O. F. Vyvenko, M. Kittler, T. Wilhelm, and M. Reiche, "A pure 1.5 mu m electroluminescence from metal-oxide-silicon tunneling diode using dislocation network," *Appl. Phys. Lett.*, vol. 93, no. 4, pp. 041108-1–041108-3, Jul. 2008.

[12] M. Kittler, X. Yu, T. McHedlidze, T. Arguirov, O. F. Vyvenko, W. Seifert, M. Reiche, T. Wilhelm, M. Seibt, O. Voss, A. Wolff, and W. Fritzsche, "Regular dislocation networks in silicon as a tool for nanostructure devices used in optics, biology, and electronics," *Small*, vol. 3, no. 6, pp. 964–973, Jun. 2007.

[13] C. L. Hsin, W. W. Wu, L. W. Chu, H. C. Hsu, and L. J. Chen, "Controlled growth of the silicide nanostructures on Si bicrystal nanotemplate at a precision of a few nanometres," *CrystEngComm*, vol. 13, no. 12, pp. 3967–3970, Jun. 2011.

[14] C. L. Hsin, C. W. Huang, C. H. Cheng, H. S. Teng, and W. W. Wu, "Shape control of nickel silicide nanocrystals on stress-modified surface," *CrystEngComm*, vol. 16, no. 9, pp. 1611–1614, Mar. 2014.

[15] K. Rousseau, J. L. Rouviere, F. Fournel, and H. Moriceau, "Stability of interfacial dislocations in (001) silicon surfacial grain boundaries," *Appl. Phys. Lett.*, vol. 80, no. 22, pp. 4121–4123, Jun. 2002.

[16] P. E. J. Eriksson, K. Sakamoto, and R. I. G. Uhrberg, "Electronic structure of the thallium-induced 2×1 reconstruction on Si(001)," *Phys. Rev. B*, vol. 81, no. 20, pp. 205422–1–205422-5, May 2010.

[17] K. Yasui and J. Kanasaki, "Scanning tunneling microscopic studies of laser-induced modifications of Si(001)-(2×1) surface," *J. Appl. Phys.*, vol. 110, no. 10, pp. 103516-1–103516-5, Nov. 2011.

[18] C. P. Chang, M. W. Chu, H. T. Jeng, S. L. Cheng, J. G. Lin, J. R. Yang, and C. H. Chen, "Condensation of two-dimensional oxide-interfacial charges into one-dimensional electron chains by the misfit-dislocation strain field," *Nature Commun.*, vol. 5, pp. 3522–1–3522-8, Mar. 2014.

[19] M. S. Xu, S. Tsukamoto, S. Ishida, M. Kitamura, Y. Arakawa, R. G. Endres, and M. Shimoda, "Conductance of single thiolated poly(GC)-poly(GC) DNA molecules," *Appl. Phys. Lett.*, vol. 87, no. 8, pp. 083902-1–083902-3, Aug. 2005.

[20] J. W. G. Wildoer, L. C. Venema, A. G. Rinzler, R. E. Smalley, and C. Dekker, "Electronic structure of atomically resolved carbon nanotubes," *Nature*, vol. 391, no. 6662, pp. 59–62, Jan. 1998.

[21] S. Shallcross, S. Sharma, and O. Pankratov, "Emergent momentum scale, localization, and van Hove singularities in the graphene twist bilayer," *Phys. Rev. B*, vol. 87, no. 24, pp. 245403-1–245403-10, Jun. 2013.

[22] X. Zhang and H. Luo, "Scanning tunneling spectroscopy studies of angle-dependent van Hove singularities on twisted graphite surface layer," *Appl. Phys. Lett.*, vol. 103, no. 23, pp. 231602-1–231602-5, Dec. 2013.

[23] M. Kittler, X. Yu, O. F. Vyvenko, M. Birkholz, W. Seifert, M. Reiche, T. Wilhelm, T. Arguirov, A. Wolff, W. Fritzsche, and M. Seibt, "Self-organized pattern formation of biomolecules at silicon surfaces: Intended application of a dislocation network," *Mater. Sci. Eng. C*, vol. 26, no. 5–7, pp. 902–910, Jul. 2006.

[24] V. Milman, B. Winkler, J. A. White, C. J. Pickard, M. C. Payne, E. V. Akhmatskaya, and R. H. Nobes, "Electronic structure, properties, and phase stability of inorganic crystals: A pseudopotential plane-wave study," *Int. J. Quantum Chem.*, vol. 77, no. 5, pp. 895–910, Apr. 2000.

[25] M. C. Payne, M. P. Teter, D. C. Allan, T. A. Arias, and J. D. Joannopoulos, "Iterative minimization techniques for ab initio total-energy calculations-molecular-dynamics and conjugate gradients," *Rev. Mod. Phys.*, vol. 64, no. 4, pp. 1045–1097, Oct. 1992.

[26] D. Vanderbilt, "Soft self-consistent pseudopotnetials in a generalized eigenvalue formalism," *Phys. Rev. B*, vol. 41, no. 11, pp. 7892–7895, Apr. 1990.

[27] J. P. Perdew, J. A. Chevary, S. H. Vosko, K. A. Jackson, M. R. Pederson, D. J. Singh, and C. Fiolhais, "Atoms, molecules, solids, and surface—Applications of the generalized gradient approximation for exchange and correlation," *Phys. Rev. B*, vol. 46, no. 11, pp. 6671–6687, Sep. 1992.

[28] J. P. Perdew and Y. Wang, "Accurate and simple analytic representation of the electron-gas correlation-energy," *Phys. Rev. B*, vol. 45, no. 23, pp. 13244–13249, Jun. 1992.